Construction and Building Materials 438 (2024) 136974

Contents lists available at ScienceDirect

Construction and Building Materials

journal homepage: www.elsevier.com/locate/conbuildmat

Mechanical properties of basalt macro fibre reinforced geopolymer concrete

Zhijie Huang [a], Cek Sem So [a], Wensu Chen [a,*], Paing Min Htet [a], Hong Hao [b,a,**]

[a] Center for Infrastructural Monitoring and Protection, School of Civil and Mechanical Engineering, Curtin University, Australia
[b] Earthquake Engineering Research & Test Center, Guangzhou University, China

ARTICLE INFO

Keywords:
Geopolymer concrete (GPC)
Basalt macro fibres (BMFs)
Mechanical properties
Compressive tests
Flexural tests

ABSTRACT

Growing public environmental awareness leads to an increased focus on utilizing green and sustainable materials in infrastructure construction. Geopolymer concrete (GPC) and basalt macro fibres (BMFs) are promising construction materials due to their eco-friendly merits and excellent mechanical properties. In this study, a new type of BMFs reinforced GPC (BMF-GPC) was developed, and the compressive and flexural properties of BMF-GPC were investigated. The effects of BMF content and length on the mechanical properties of GPC were studied. It was found that with the addition of 2 % BMFs, the compressive and flexural toughness (energy absorption capacities) of GPC were greatly enhanced by up to 126 % and 965 %, respectively. Increasing the content and length of BMFs resulted in favourable outcomes for strain softening of GPC under compression and post-cracking behaviour of GPC under flexural loads, whilst having limited effects on the modulus of elasticity and flexural strength. Additionally, an analytical model was proposed to predict the compressive stress-strain behaviour of BMF-GPC, which could be used for the design of BMF-GPC structures.

1. Introduction

With the growing public environmental awareness, there is an increasing trend towards using more sustainable materials in infrastructure construction, such as geopolymer concrete (GPC) and basalt fibres [1]. GPC is a type of concrete that utilises industrial wastes such as fly ash and slag as alternative binder materials to cement, resulting in fewer carbon emissions whilst maintaining competitive mechanical properties as compared to ordinary Portland cement concrete (OPC) [2–4]. Basalt fibre is a type of inorganic fibre for reinforcing concrete, which is environmentally friendly and sustainable due to its natural material resources (made from natural basalt rock) [5]. In addition, basalt fibres have other merits such as low cost, high tensile strength, high temperature resistance, good corrosion resistance to water, salt, and acid, etc. [6,7]. The integration of these two materials benefits infrastructure construction due to their green and sustainable attributes.

However, there is a concern about the alkali resistance of basalt fibres in concrete as concrete matrix exhibits a strong alkaline environment. It is reported that traditional basalt fibres have low corrosion resistance to alkali [7,8]. As compared to traditional basalt fibres, basalt macro fibres (BMFs) have much higher durability in alkaline environments [8]. BMFs are a type of novel fibres that consist of bundled basalt fibres embedded into a resin matrix, forming mini basalt fibre-reinforced polymer (BFRP) bars with a diameter of approximately 0.7–1.0 mm [9]. The resin matrix plays a role in protecting the internal micro basalt fibres from chemical corrosion whilst inheriting the advantages of basalt fibres [10]. Nowadays, BMFs have become a popular choice among various fibres for reinforcing concrete [11–13].

In recent years, some efforts have been made to explore the mechanical properties of BMFs reinforced concrete (BMF-C). Currently, there is no consensus on the effect of BMFs on the compressive strength of concrete. Tests by Branston et al. [9] and Wang et al. [11] showed that the addition of BMFs with a content of 0.31–2 % by volume fraction led to a 31–45 % lower compressive strength of concrete. On the contrary, tests by Sohail et al. [14] and Alnahhal et al. [15] found that the addition of BMFs with a volume fraction of 0.25–1 % slightly improved the compressive strength of concrete by 6.2–17.5 %. Meanwhile, some tests by Adhikari [16] and Zhang et al. [17] showed that the inclusion of BMFs with a content of 0.5–1.5 % had an insignificant effect on the compressive strength of concrete, and so did the elastic modulus. As for

* Corresponding author.
** Corresponding author at: Earthquake Engineering Research & Test Center, Guangzhou University, China.
E-mail addresses: wensu.chen@curtin.edu.au (W. Chen), hong.hao@curtin.edu.au (H. Hao).

https://doi.org/10.1016/j.conbuildmat.2024.136974
Received 18 April 2024; Received in revised form 4 June 2024; Accepted 5 June 2024
Available online 15 June 2024

the splitting and flexural strength of concrete, studies demonstrated that adding BMFs with a content of 1–1.5 % could enhance the flexural strength by up to 17–23 % [14,15] and splitting tensile strength by 16 % [17]. More importantly, the post-cracking behaviour and flexural toughness were also improved with the addition of BMFs [18]. Some studies also investigated the effect of BMFs on the performance of concrete with different sustainable aggregates, e.g., steel slag aggregates and gravel aggregates [15], recycled concrete aggregates [14,19], lightweight aggregates [10], etc., and other types of concrete such as high performance concrete [18,20] and ultra-high performance concrete (UHPC) [21,22].

A good understanding of the mechanical properties of BMF-GPC could facilitate predicting its structural behaviour, enabling effective designs. However, very few studies on BMF-GPC have been reported in the open literature to date. Only one study [23] carried out tests on BMFs reinforced fly ash-based geopolymer composites (without sand and coarse aggregates), with the fibre volume fraction ranging from 12.5 % to 75 %. The results showed that the geopolymer composites with BMFs had 12–26 times higher flexural strength and 4–8 times higher tensile strength than those without fibres, owing to the high percentage of volume fraction of BMFs. It should be noted that the specimens were very small (2 × 2 × 7 cm), and the BMFs served as longitudinal reinforcements rather than fibres. In this study, compressive and flexural tests were conducted to reveal the mechanical properties of BMF-GPC. The slump, modulus of elasticity, compressive strength, compressive stress-strain curves, flexural strength, and flexural toughness of BMF-GPC were obtained and analysed.

2. Experimental programme

In this section, the details of the experimental program are presented, covering the raw materials used in BMF-GPC, the mix design, and the testing methods. The raw materials used in BMF-GPC include binder materials, activators, aggregates, and BMFs. Subsequently, the mix designs are outlined, specifying the weight proportions of each type of raw material. Lastly, the tests conducted are described, along with the respective standards followed in the tests.

2.1. Raw materials

Commercially available Class F fly ash compliant with AS/NZS 3582.1 [24] (Grade I) and ground granulated blast-furnace slag (GGBFS) conforming to AS 3582.2 [25] were used as binder materials. Table 1 gives the details of chemical compositions and loss on ignition of fly ash and GGBFS [26]. The alkali activators consisted of a commercially available D grade sodium silicate (Na_2SiO_3) solution and a sodium hydroxide (NaOH) solution with a concentration of 12 Molarity. Crushed granite was used as coarse aggregates, which comprised two different maximum nominal sizes, i.e., 7 mm and 10 mm (each accounted for 50 % of the total weight), and natural sand was employed as fine aggregates with a nominal maximum size of 1.2 mm. Fig. 1 shows the BMFs used for reinforcing GPC in the present study, with three different lengths, i.e., 50 mm, 35 mm, and 20 mm. Their density, diameter, tensile strength, and modulus of elasticity are 2,000 kg/m^3, 0.65 mm, 1, 200 MPa, and 50 GPa, respectively [12].

Table 1
Chemical compositions and loss on ignition of fly ash and GGBFS [26].

Chemical compositions	Fly ash (wt%)	GGBFS (wt%)
SiO_2	55.90	32.72
Al_2O_3	26.94	13.37
Fe_2O_3	0.06	0.83
CaO	4.25	41.46
MgO	1.51	5.54
MnO	0.10	0.20
TiO_2	1.43	0.60
V_2O_5	-	-
SO_3	0.20	4.97
P_2O_5	0.50	0.01
K_2O	0.76	0.30
Na_2O	0.31	0.27
SrO	-	0.12
BaO	-	-
Cr_2O_3	-	0.02
Loss on ignition	1.51	0.15

2.2. Mix design

Table 2 tabulates the weight proportions of the mixes, which followed a similar GPC mix in the authors' previous study [12]. The effects of two factors, i.e., fibre content (by volume fraction) and fibre length, were investigated. The previous studies [9,17] indicate a dosage of BMFs over 40 kg/m^3 is not favourable due to the fibre balling and compaction issues. Therefore, a maximum dosage of 40 kg/m^3 of BMFs was selected in this study, corresponding to a fibre content of 2 % by volume fraction. Mix 1 (M1) without fibres serves as a benchmark for other mixes. The effect of fibre content was investigated through three mixes (M1, M2, and M3) with volume fractions of 0, 1 %, and 2 %, respectively. In previous studies [17, 20, 23, 27], fibre lengths ranging from 18 mm to 55 mm were commonly used. In this study, three different lengths of 20 mm (M4), 35 mm (M2), and 50 mm (M5) were chosen to evaluate the effect of fibre length.

2.3. Testing methods

Concrete specimens were cast and cured for 28 days under ambient conditions. Slump tests were conducted according to ASTM C143 [28]. Cylinders with a diameter of 100 mm and a height of 200 mm were prepared to determine the modulus of elasticity and compressive strength. Compressive tests were conducted as per ASTM C39 [29], as shown in Fig. 2(a). It is required that the load shall be applied continuously at a specified loading rate not exceeding 0.25 MPa/s. Therefore, a loading rate of 0.08 MPa/s was applied in this study. Tests on modulus of elasticity were carried out in accordance with ASTM C469 [30]. Flexural tests with a four-point bending configuration were performed following ASTM C1609 [31]. Prisms with a cross-sectional size of 100 × 100 mm and a length of 400 mm, consistent with the specimen dimension in previous studies [32,33], were prepared for the flexural tests, as shown in Fig. 2(b). The span (L) between the two support rollers was 300 mm. A loading rate of 0.075 mm/min was initially applied until reaching a net deflection of $L/9$ (0.33 mm). After that, it was changed to 0.5 mm/min, in accordance with the provisions (not exceeding 8 times the initial rate) of ASTM C1609 [31].

3. Results and analysis

3.1. Workability

The slumps of all mixes were measured to evaluate the workability of BMF-GPC, which is presented in Fig. 3. All mixes exhibited slumps in the range of 140–220 mm, which is similar to the slump range (125–200 mm) of BMF-C reported in reference [34]. The higher BMF content resulted in a lower slump of BMF-GPC. However, increasing the

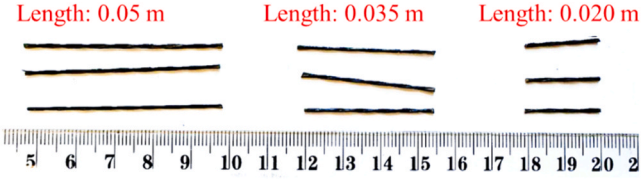

Fig. 1. Pictures of basalt macro fibres (BMFs) used in this study.

Table 2
Mix design of the BMF-GPC.

Mix No.	CA (kg/m^3)	FA (kg/m^3)	Binders (kg/m^3)		Solutions (kg/m^3)		BMFs (kg/m^3)	Fibre content (%)	Fibre length (mm)
			Fly ash	GGBFS	Na_2SiO_3	NaOH			
M1	1220	650	280	120	129	51	0	**0**	**0**
M2	1220	650	280	120	129	51	20	**1**	**35**
M3	1220	650	280	120	129	51	40	**2**	35
M4	1220	650	280	120	129	51	20	1	**20**
M5	1220	650	280	120	129	51	20	1	**50**

Note: "CA": Coarse Aggregates; "FA": Fine Aggregates; "GGBFS": ground granulated blast-furnace slag; "BMF": Basalt Macro Fibres.

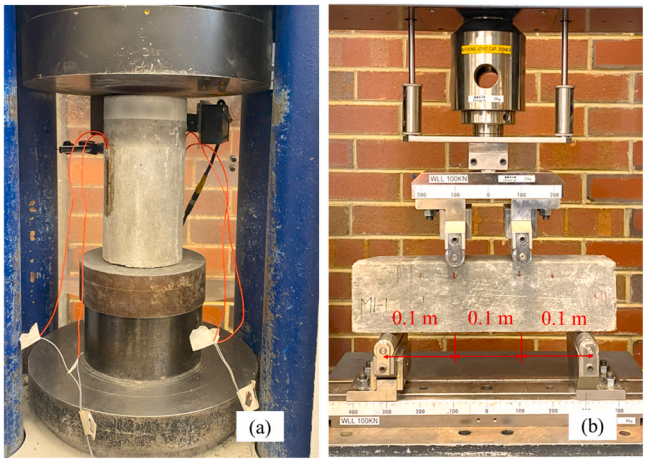

Fig. 2. Configuration of tests: (a) compressive tests and (b) flexural tests.

BMF length from 20 mm to 50 mm with 1 % content only slightly reduced the slump of BMF-GPC by 6 %. The effect of BMF length on the slump of BMF-GPC is negligible.

3.2. Modulus of elasticity

The moduli of elasticity of specimens are shown in Fig. 4. Statistical analysis on the modulus of elasticity was also conducted via *t*-test [35]. A p-value of less than 0.05 from *t*-tests is usually considered statistically significant [36]. For instance, the p-value between specimens with 0 % and 2 % BMFs is 0.0004 (less than 0.05) from *t*-tests, which is considered statistically significant. The average modulus of elasticity of GPC specimens decreased by 18 % (from 24.5 GPa to 20.0 GPa, as shown in Fig. 4 (a)), which indicates the clear effect of increasing BMF content from 0 % to 2 % on the modulus of elasticity. Meanwhile, the average moduli of elasticity of GPC specimens with 0 % and 1 % BMFs are 24.5 GPa and 23.8 GPa, respectively. The corresponding p-value between the specimens with 0 % and 1 % BMFs is 0.375 (higher than 0.05) from *t*-tests, which is considered statistically nonsignificant and indicates the insignificant effect of increasing BMF content from 0 % to 1 % on the

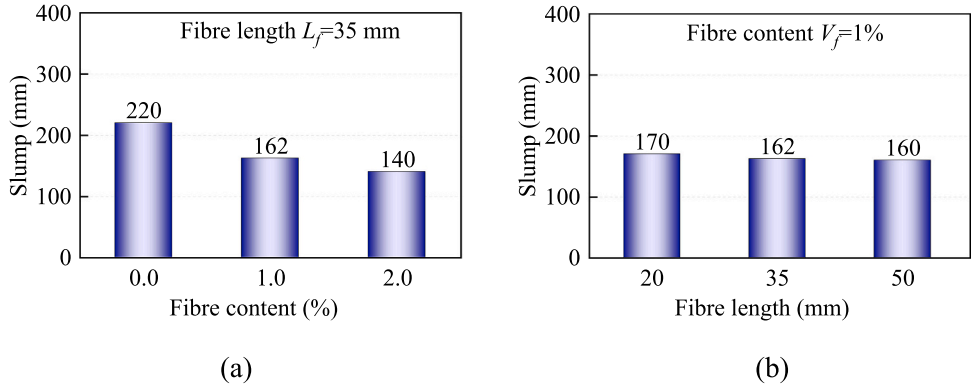

Fig. 3. Effects of (a) fibre content and (b) fibre length on the workability of GPC.

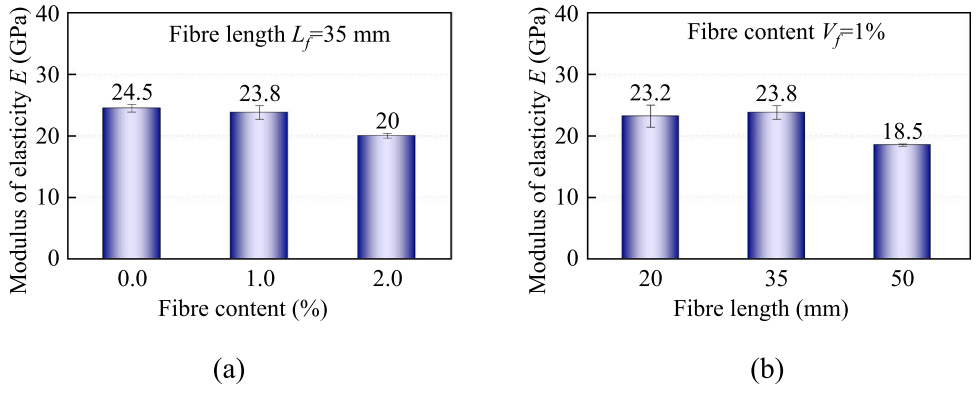

Fig. 4. Effects of (a) fibre content and (b) fibre length on the modulus of elasticity of GPC.

modulus of elasticity of GPC. Specimens with different fibre lengths generally had a similar modulus of elasticity, except for M5, which had a relatively lower modulus of elasticity due to the lower compressive strength of concrete (presented in Section 3.3.1).

To exclude the effect of compressive strength variation among different batches, the normalised moduli of elasticity [37–39] of the specimens are shown in Fig. 5, which were calculated by dividing the modulus of elasticity by the square root of compressive strength (f_c) of GPC, i.e., $E/(f_c)^{1/2}$, since the modulus of elasticity of concrete is linearly proportional to the square root of the compressive strength of concrete [40,41].

The relationship of the normalised modulus of elasticity versus fibre content V_f (with the same fibre length L_f of 35 mm) is shown in Fig. 5(a). The results show that the normalised modulus of elasticity of GPC decreased by up to 12 % with the increase in fibre content by up to 2 %, indicating that fibre content (0–2 %) has a limited effect on the modulus of elasticity of GPC. The formula of the normalised modulus of elasticity ($E/(f_c)^{1/2}$) of BMF-GPC as a function of fibre content (V_f) can be fitted as Eq. (1) below.

$$\frac{E}{f_c^{\frac{1}{2}}} = -20636.0V_f + 3353.8, \quad 0 \le V_f \le 2\%, \quad L_f = 35mm \tag{1}$$

The relationship of the normalised modulus of elasticity versus fibre length L_f (with the same fibre content V_f of 1 %) is given in Fig. 5(b). It shows that the normalised modulus of elasticity of GPC decreased by 12 % with increasing fibre length from 20 mm to 50 mm, indicating that fibre length (20–50 mm) has a limited effect on the modulus of elasticity of GPC. The formula of the normalised modulus of elasticity ($E/(f_c)^{1/2}$) of BMF-GPC as a function of fibre length (L_f) is fitted as Eq. (2).

$$\frac{E}{f_c^{\frac{1}{2}}} = -12.9L_f + 3554.6, \quad 20 \le L_f \le 50\text{mm}, \quad V_f = 1\% \tag{2}$$

3.3. Compressive tests

3.3.1. Compressive strength

The compressive strengths of specimens from each mix are presented in Fig. 6. Overall, the GPC specimens with different fibre contents (V_f) exhibit similar compressive strengths ranging from 46.6 MPa to 56.1 MPa. This observation is consistent with that reported in references [16–18] for OPC. The GPC specimens with different fibre lengths (L_f) also exhibit compressive strength within the range of 41.3–56.1 MPa, whereas the specimens (M5) with 50 mm-long BMFs have a relatively lower strength of 41.3 MPa. This might be attributed to more lacunas or voids formed in the GPC matrix of M5 specimens with BMFs because longer fibre length could cause more difficulties for concrete consolidation as reported in reference [9]. Strength variations of GPC were also reported in previous studies [42–44]. It is worth mentioning that a fibre content higher than 2 % might lead to fibre balling and compaction difficulties [9, 17], resulting in decreased strength.

3.3.2. Compressive stress-strain relation

The effect of fibre content on the compressive stress-strain behaviour of the GPC specimens is illustrated in Fig. 7. It should be noted that the data of specimen M1–3 from Batch M1 was not obtained due to the malfunction of the testing machine. It is observed that GPC specimens without fibres (M1) failed in a very brittle manner, indicated by a sudden decrease in compressive stress after reaching the peak stress. For specimens (M2) with 1 % fibre content, the compressive stress gradually decreased after the peak stress. With a fibre content of 2 % (M3), GPC specimens showed a more ductile strain softening stage after the peak stress. The test results indicate that higher BMF content leads to more ductile post-peak compressive softening behaviour of GPC. The peak strain ε_0 (the strain corresponding to the peak stress) is shown in Fig. 7 (d). The mean peak strains $\varepsilon_{0,m}$ of the specimens with fibre contents of 0, 1 %, and 2 % and a fibre length of 35 mm are 2,734 με, 3,087 με, and 3,458 με, respectively. It shows that the peak strain ε_0 is linearly proportional to the fibre content, with the equation presented below.

$$\varepsilon_0 = 36200V_f + 2731, \quad 0 \le V_f \le 2\%, \quad L_f = 35mm \tag{3}$$

The effect of fibre length on the compressive stress-strain behaviour of GPC is shown in Fig. 8. Both the specimens without fibres (M1) and those with 20 mm-long fibres (M4) exhibited brittle failure with an abrupt decrease in post-peak compressive stress, except for the tail stage of the M4 specimens. This suggests that the addition of 1 % fibre content with a length of 20 mm has a negligible effect on the compressive stress-strain behaviour of GPC. As the fibre length increased to 35 mm and 50 mm, a more ductile compressive stress-strain behaviour of the specimens was observed, characterised by decreasing slopes of the curves. Fig. 8(e) provides the peak strains ε_0 of the specimens with different fibre lengths. It can be found that increasing the fibre length from 20 mm to 50 mm almost led to a linear increase in the peak strains ε_0, as given in Eq. (4).

$$\varepsilon_0 = 24.9L_f + 2236, \quad 20 \le L_f \le 50\text{mm}, \quad V_f = 1\% \tag{4}$$

3.3.3. Compressive toughness and index

The toughness of concrete under compression (T_c), also referred to as energy absorption, is defined as the area under the stress-strain curve up to a specified strain value [45, 46]. The compressive toughness index (I_c) is defined as the ratio of the toughness of fibre-reinforced concrete to that of plain concrete [47]. In this study, a specified strain value of 9,000 με was used for the toughness calculation, where the corresponding compressive stress decreased to a very low value, e.g., 5–6 MPa. It should be noted that the stress-strain curves of M4 specimens did not reach 9,000 με, as shown in Fig. 8(b), due to the termination of compressive tests. The toughness of M4 specimens up to a strain value of 9,000 με was then calculated with the extended stress-strain curves

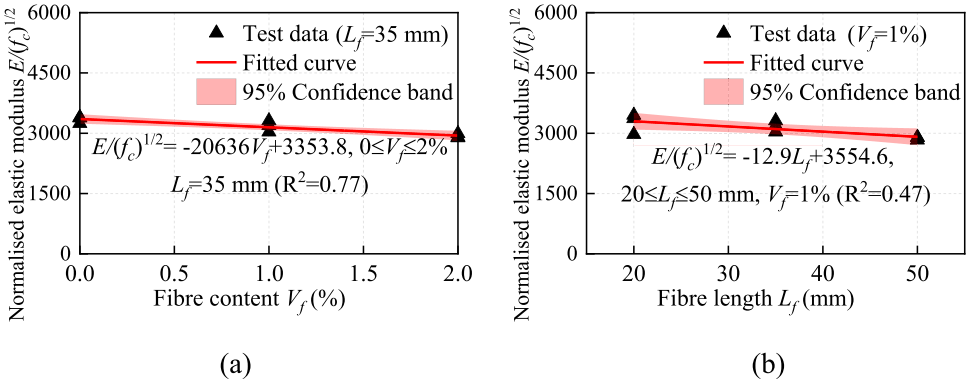

Fig. 5. Effects of (a) fibre content and (b) fibre length on the normalised modulus of elasticity of GPC.

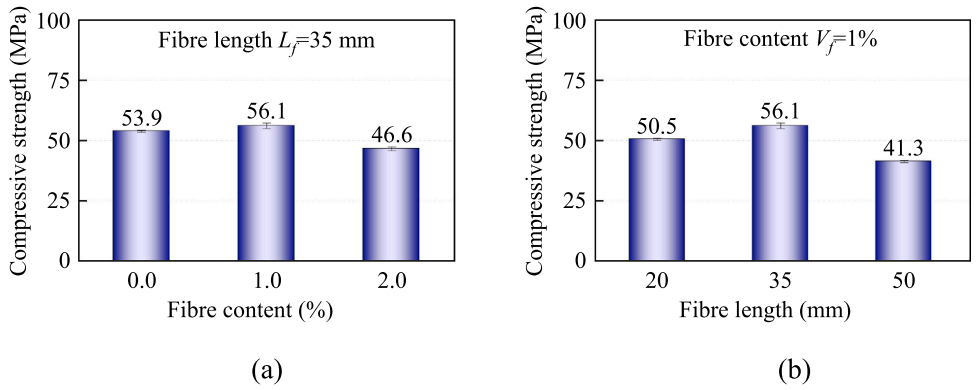

Fig. 6. Effects of (a) fibre content and (b) fibre length on the compressive strength of GPC.

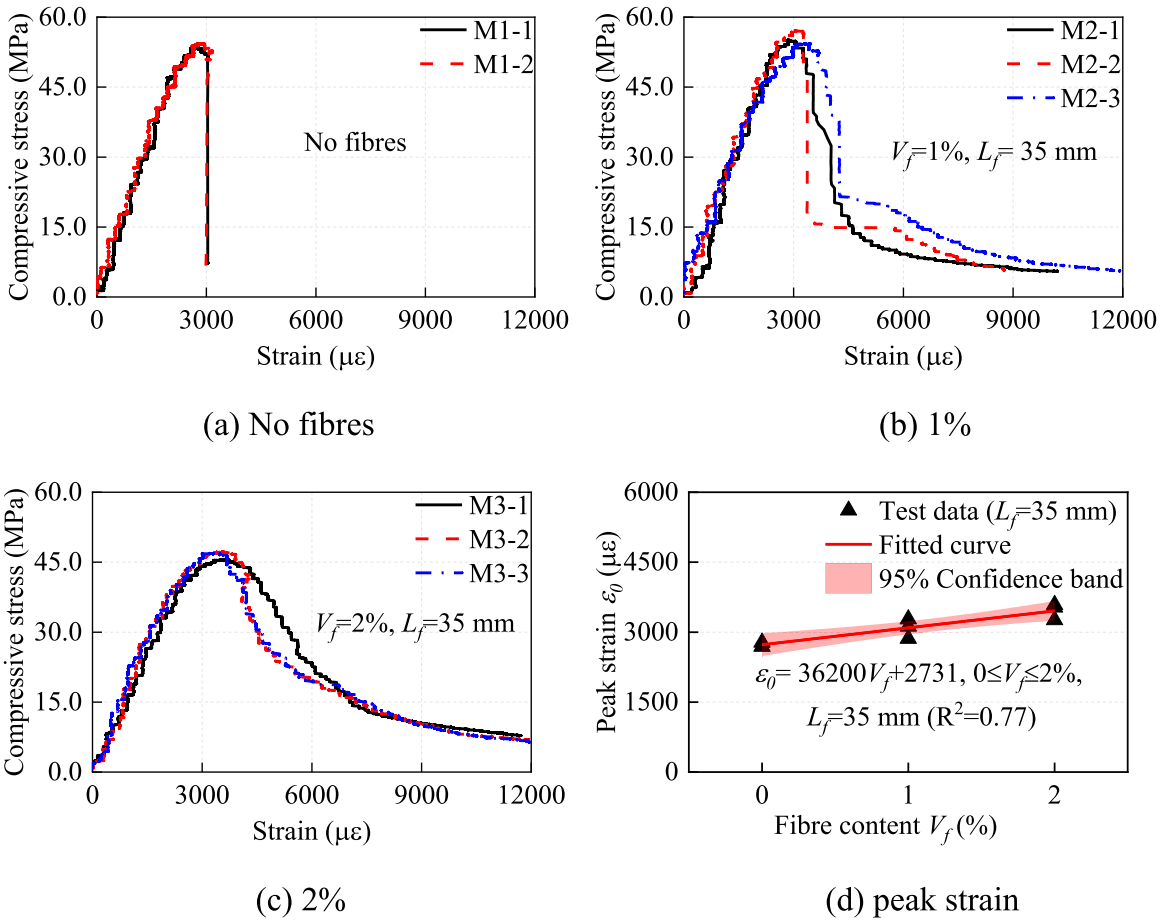

Fig. 7. Effect of fibre content on the compressive stress-strain behaviour of GPC (for L_f=35 mm).

assumed to be horizontal lines, since the slopes of the curves at the tail stage are almost 0 as shown in Fig. 8(b). The compressive toughness (T_c) of the specimens is shown in Fig. 9(a) and (c). As observed, the addition of BMFs significantly enhanced the toughness of GPC. Higher BMF content and longer fibre length led to increased toughness. As compared to plain GPC, the addition of BMFs up to 2 % resulted in improved compressive toughness by up to 126 %, and a BMF length up to 50 mm achieved higher compressive toughness by up to 99 %. Similarly, the compressive toughness index I_c also increased with fibre content and length, as shown in Fig. 9(b) and (d). It should be noted that the compressive toughness and index of specimens with 50 mm-long fibres (M5) are slightly lower than those of specimens with 35 mm-long fibres (M2), due to the lower compressive strength of M5 specimens as mentioned in Section 3.3.1.

3.4. Proposed analytical model for compressive stress-strain behaviour

In the past decades, various analytical models [46, 48–53] have been proposed for predicting the compressive stress-strain behaviour of concrete and fibre-reinforced concrete. Among these models, the expression of Eq. (5), proposed by Popovics [48], is widely selected as a basic form for other models [49–51], where the normalised stress σ/f_c is a function of the normalised strain $\varepsilon/\varepsilon_0$ and β (a material parameter). The material parameter β could be obtained through regression analysis of the test results, considering the effects of independent variables such as fibre content and fibre length.

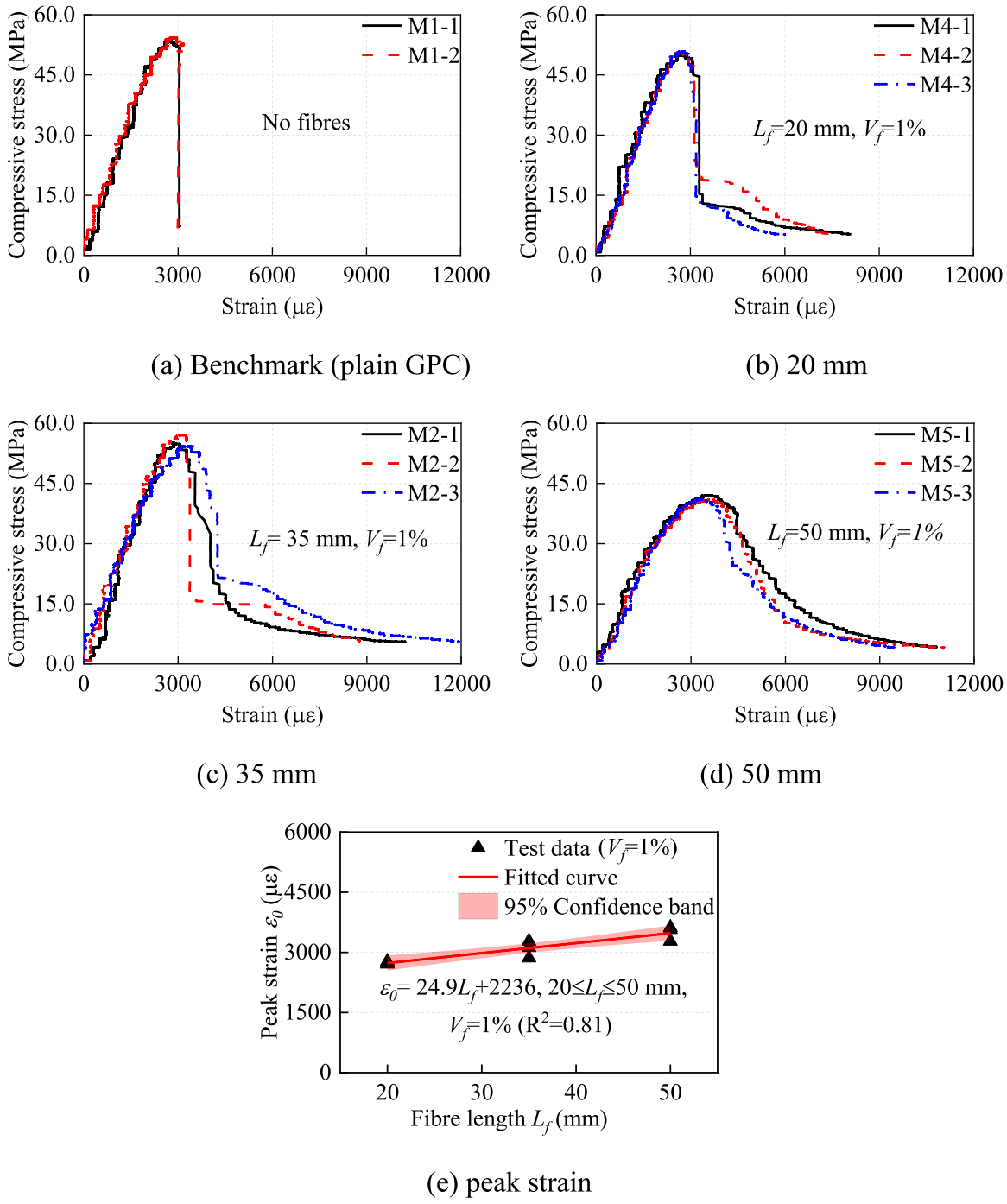

Fig. 8. Effect of fibre length on the compressive stress-strain behaviour of GPC (for V_f=1 %).

$$\frac{\sigma}{f_c}=\frac{\beta\frac{\varepsilon}{\varepsilon_0}}{\beta-1+\left(\frac{\varepsilon}{\varepsilon_0}\right)^{\beta}} \quad (5)$$

In this study, the effects of both fibre content (V_f, by volume fraction) and fibre length (L_f) on the compressive stress-strain behaviour of GPC were investigated. Subsequently, a reinforcing index (*RI*), defined as Eq. (6), is used to combine the effects of both fibre content (V_f) and fibre length (L_f), which has been widely used for fibre-reinforced concrete [50, 54, 55]. In Eq. (6), d_f represents the diameter of BMFs, which is 0.65 mm as mentioned in Section 2.1. Thus, the reinforcing indices (*RI*s) of M1 to M5 are calculated as 0, 0.54, 1.08, 0.31, and 0.77, respectively.

$$RI=\frac{V_f L_f}{d_f} \quad (6)$$

Subsequently, the effect of reinforcing index (*RI*) on the normalised stress-strain curves of the GPC specimens is illustrated in Fig. 10. One representative specimen from each mix is shown. As seen, the ascending branches of the normalised stress-strain curves are generally consistent, while the descending branches are significantly different. With a higher reinforcing index *RI*, the post-peak strain softening phase of the compressive stress-strain curves of GPC becomes more ductile. This again confirms the conclusion stated above that higher fibre content and longer fibre length lead to a more ductile compressive stress-strain behaviour and higher toughness of GPC.

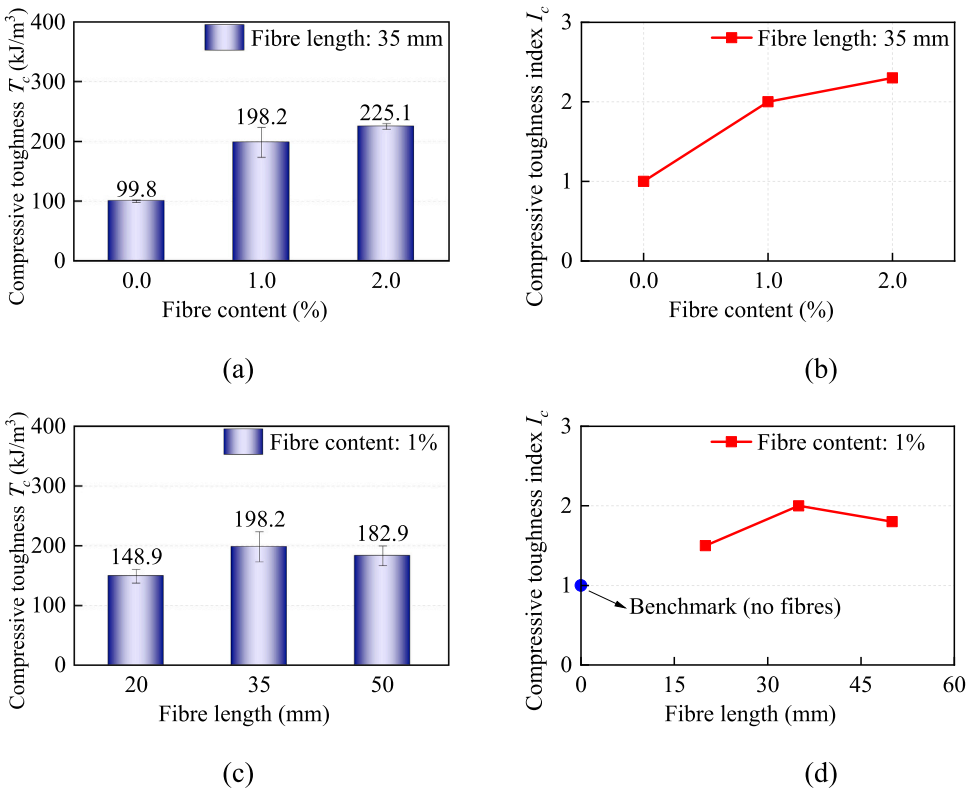

Fig. 9. Effects of fibre content ((a) & (b)) and fibre length ((c) & (d)) on the compressive toughness T_c and compressive toughness index of GPC specimens.

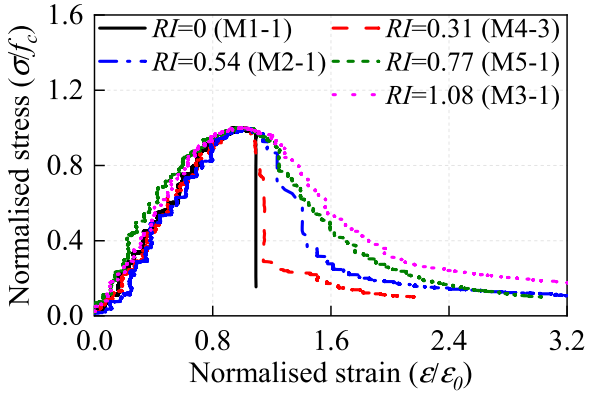

Fig. 10. Effect of reinforcing index (*RI*) on the normalised stress-strain behaviour of the GPC specimens.

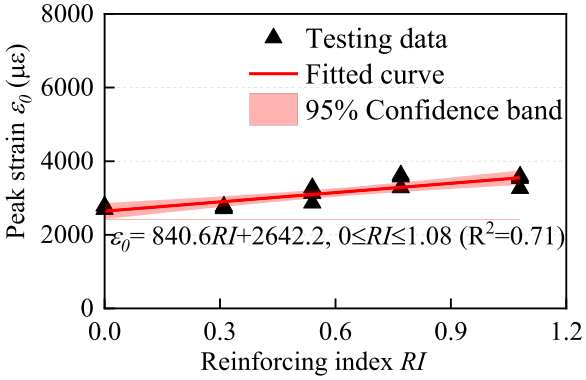

Fig. 11. Effect of reinforcing index *RI* on the peak strain ε_0 of the GPC specimens.

Through regression analysis, the material parameter β can be obtained as a function of the reinforcing index (*RI*), as given in Eq. (7). Given the specific values of compressive strength of concrete f_c, BMF content (V_f), and fibre length (L_f), the compressive stress-strain curve of BMF-GPC could be calculated using Eqs. (5)-(7), provided the peak strain ε_0 (the strain corresponding to the peak stress f_c) is known. Therefore, it is necessary to find an explicit relationship between the peak strain ε_0 and the reinforcing index (*RI*). Fig. 11 shows the effect of reinforcing index *RI* on the peak strain, giving a linear relationship between the peak strain ε_0 and the reinforcing index (*RI*), as presented in Eq. (8). Eventually, the compressive stress of BMF-GPC at a given strain could be predicted via Eqs. (5)-(8). The comparison of the compressive stress-strain curves between the test results and the proposed analytical model in the present study is shown in Fig. 12. It can be seen that the proposed analytical model in this study could well predict the compressive strain-stress behaviour of GPC with and without BMFs, which can be used for the design of BMF-GPC structures in the future.

$$\beta = 26.3e^{-1.63RI} \tag{7}$$

$$\varepsilon_0 = (840.6RI + 2642.2) \times 10^{-6} \tag{8}$$

3.5. Flexural tests

3.5.1. Failure modes

The failure modes and cracking surface of the specimens in flexural tests are shown in Fig. 13. As seen from the cracking surface, BMFs exhibited the main failure mode of fibre pull-out, which could lead to a gradual decrease of the post-cracking load with increasing deflection. As a result, specimens with fibres (M2-M5) experienced a ductile load-deflection behaviour as presented in Section 3.5.2. Specimens (M1) without fibres experienced very narrow flexural cracks on the tensile side of the beam prisms, which was due to the brittle failure behaviour

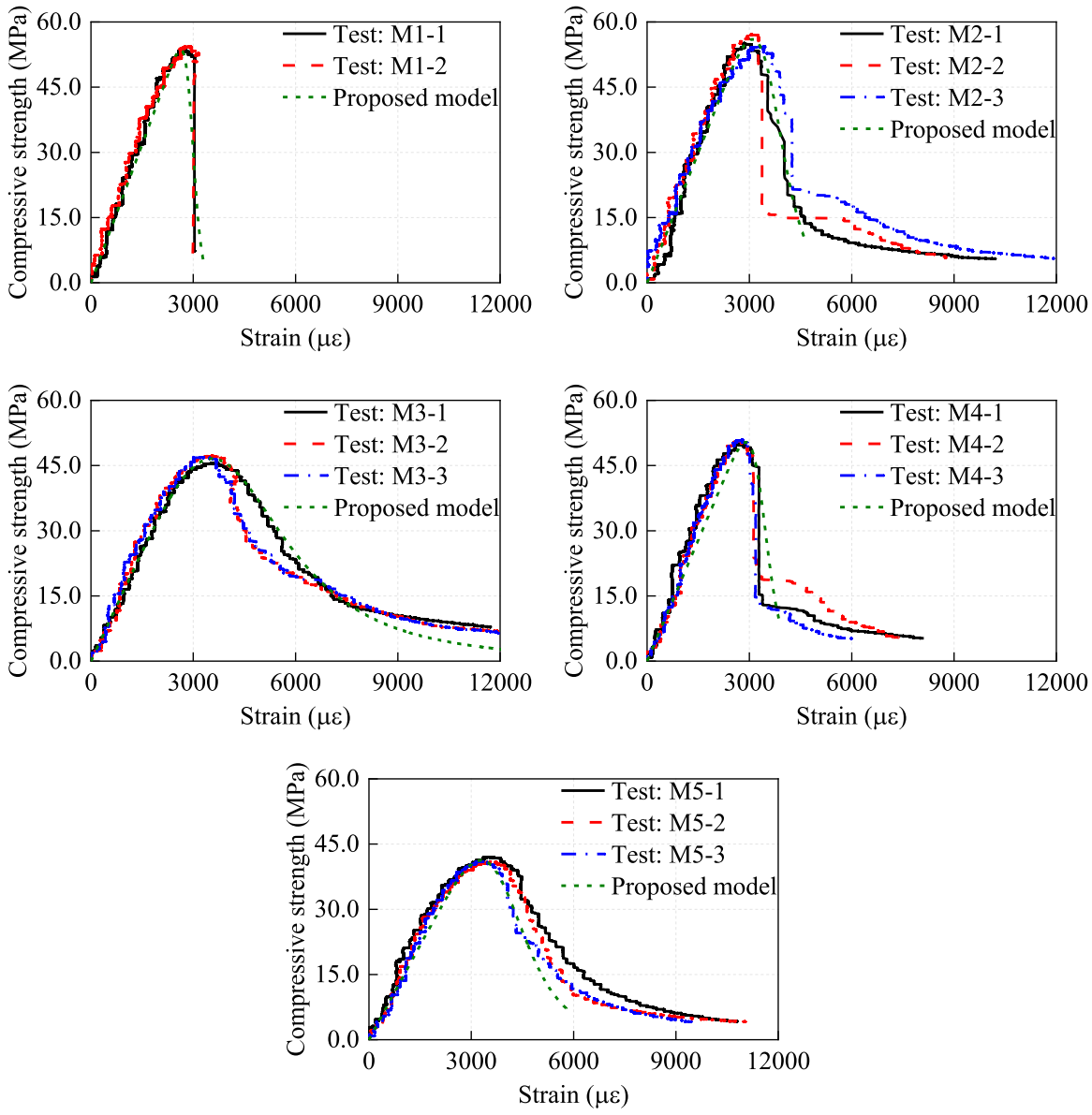

Fig. 12. Comparison of the compressive stress-strain curves between the test results and the proposed analytical model.

after cracking. The cracks of the specimens with fibres (M2-M5) are wider than those of the ones without fibres (M1) due to the improved ductility induced by the bridging effect of BMFs. Based on crack width, it can be generally known that M3 specimens have the best performance of ductility, followed by the specimens M5, M2, M4, and M1.

3.5.2. Load-deflection curves

In flexural tests, the applied load to the specimens was recorded, along with the corresponding mid-span deflection of the beam specimens. The flexural performance of concrete could be assessed by flexural strength, residual strength, flexural toughness (energy absorption), flexural toughness index, etc. A typical load-deflection curve of the specimens subjected to four-point bending is illustrated in Fig. 14, where L is the span length (300 mm) of the beam specimens between the two supports. The strength f can be obtained by using Eq. (9).

$$f = \frac{PL}{bd^2} \tag{9}$$

where P is the recorded load (including peak load P_1, post-cracking residual loads $P_{L/400}$, $P_{L/300}$, $P_{L/150}$, and $P_{L/100}$ at the corresponding deflections of $L/400$, $L/300$, $L/150$, and $L/100$, respectively), and b and d are the width (100 mm) and height (100 mm) of the beam prisms, respectively. According to ASTM C1609 [31], the peak load P_1 and residual loads ($P_{L/400}$, $P_{L/300}$, $P_{L/150}$, and $P_{L/100}$) can be used to calculate the flexural strength f_f (also named as modulus of rupture) and residual strengths ($f_{L/400}$, $f_{L/300}$, $f_{L/150}$, and $f_{L/100}$) of the GPC specimens, corresponding to a specified net deflection of $L/400$, $L/300$, $L/150$, and $L/100$, i.e., 0.75 mm, 1 mm, 2 mm, and 3 mm, respectively. A summary of the flexural test results is listed in Table 3.

The comparison of the load-deflection curves of GPC specimens with different fibre contents is shown in Fig. 15. As seen, the specimens with no fibres almost had no post-cracking resistance, indicated by a significant decrease of the load, while those with fibres could still sustain load after cracking. With a higher fibre content, GPC exhibited higher post-cracking resistance. The mean peak loads of the specimens with fibre contents of 0, 1 %, and 2 % are 16.0 kN, 17.7 kN, and 18.1 kN, respectively. The mean peak loads of the specimens slightly increased with the fibre content. It should be noted that the specimen M2–2 has a slightly lower peak load, which might be due to the introduced lacunas and voids as reported in references [32,56]. Nevertheless, the curve

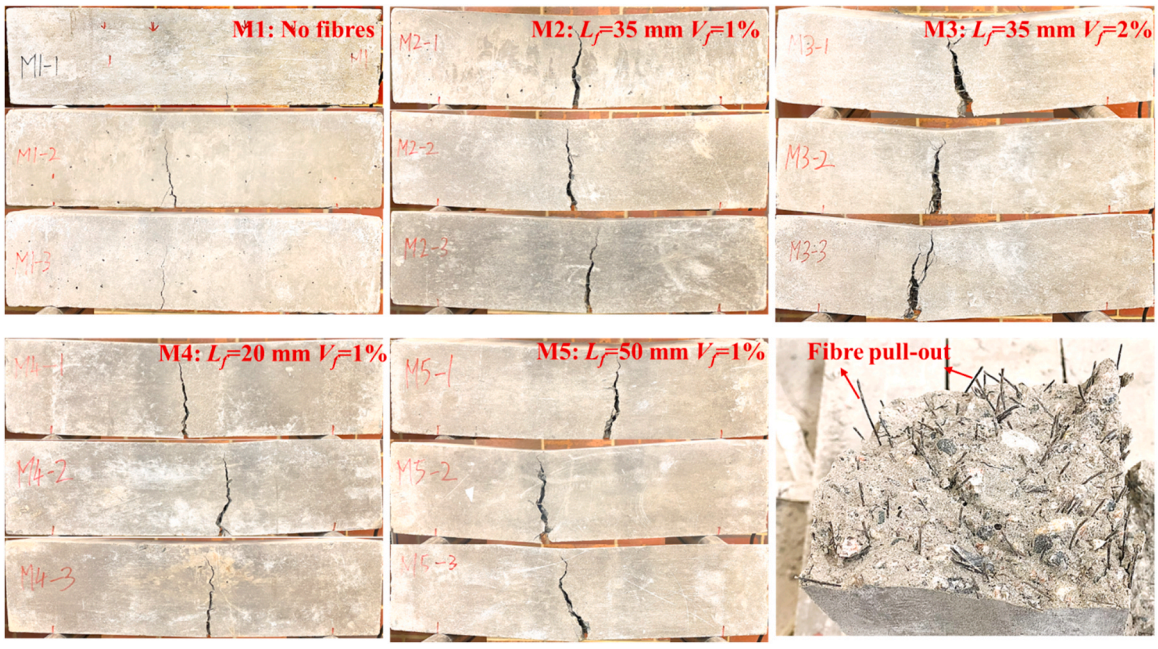

Fig. 13. Failure modes and cracking surface of the specimens under flexural loads.

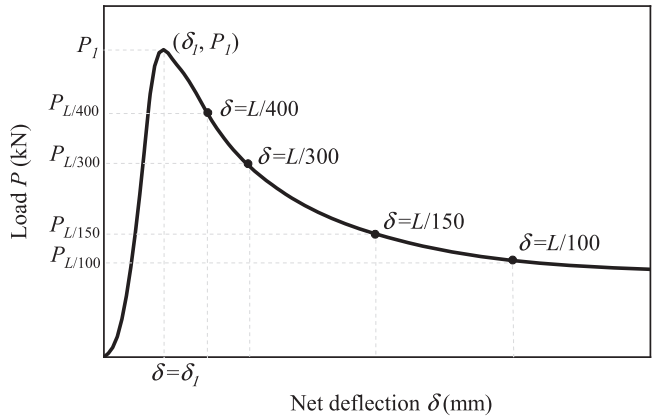

Fig. 14. Illustration of load-deflection curve of specimens from flexural tests.

profile of M2–2 is generally consistent with those of M2–1 and M2–3. The introduced lacunas and voids mainly affect the peak load, while the post-cracking behaviour is primarily governed by BMFs.

A comparison of the flexural load-deflection curves of GPC specimens with different fibre lengths is shown in Fig. 16. The peak loads of the specimens with different fibre lengths are generally similar, except for those with 50 mm-long fibres (M5) due to the lower compressive strength as mentioned in Section 3.3.1. Additionally, the specimens with longer fibres show a more ductile post-cracking behaviour than those with shorter fibres, suggesting that longer BMF length could lead to better flexural performance of BMF-GPC.

3.5.3. Flexural strength

The flexural strengths f_f of the tested specimens are shown in Fig. 17. Overall, the flexural strength of BMF-GPC is higher than that of plain GPC, except for M5 with 50 mm-long BMFs due to the lower compressive strength as mentioned in Section 3.3.1. With the increase in fibre content, the flexural strength of GPC increased, as shown in Fig. 17(a). A 2 % fibre content led to a 13 % increase in the flexural strength of GPC, indicating that BMFs have a limited effect on the flexural strength of GPC. In reference [14], test data also shows that 1 % BMFs led to a similar improvement (e.g., 17 %) in flexural strength for concrete with natural limestone aggregates. However, the flexural strength of GPC slightly decreased with the increase in fibre length, as shown in Fig. 17 (b). This trend might be attributed to a reduced number of bonding connections resulting from fewer amounts of longer fibres at the cracking section.

To exclude the effect of compressive strength, the normalised flexural strengths $f_f/(f_c)^{1/2}$ [57–59] of the specimens are shown in Fig. 18. As seen in Fig. 18(a), the normalised flexural strength also increased with fibre content. For instance, adding 2 % BMFs improved the normalised flexural strength of GPC by 22 %. The formula of the normalised flexural strength of BMF-GPC as a function of BMF volume fraction (V_f) is fitted as Eq. (10).

$$\frac{f_f}{\sqrt[2]{fc}} = 7.332V_f + 0.640, \quad 0 \le V_f \le 2\%, \quad L_f = 35mm \tag{10}$$

The relationship between the normalised flexural strength and fibre length (with the same fibre content V_f of 1 %) is shown in Fig. 18(b). It can be found that the normalised flexural strength of BMF-GPC slightly decreased with fibre length. Increasing fibre length from 20 mm to 50 mm led to a 14 % reduction in normalised flexural strength. The normalised flexural strength as a function of BMF length is given in Eq. (11).

$$\frac{f_f}{\sqrt[2]{fc}} = -0.004L_f + 0.834, \quad 20 \le L_f \le 50mm, \quad V_f = 1\% \tag{11}$$

3.5.4. Residual strength

The average residual strength of three specimens from each group is depicted in Fig. 19. The residual strength of GPC specimens without fibres is zero (black lines). As expected, the residual strength of GPC specimens decreased with deflections, owing to the reduction in concrete area at the cracking section. As shown in Fig. 19(a), GPC with 2 % BMFs had 50 %, 117 %, 343 %, and 375 % higher residual strengths than that with 1 % BMFs at the net deflections of $L/400$, $L/300$, $L/150$, and $L/100$, respectively. Fig. 19(b) shows the residual strengths of BMF-GPC with 50 mm-long BMFs were 37 %, 56 %, 146 %, and 183 % higher than those of BMF-GPC with 20 mm-long BMFs at the net deflections of $L/400$, $L/300$, $L/150$, and $L/100$, respectively. It indicates that the effect of fibre content on the residual strength of BMF-GPC is more prominent

Table 3
Summary of flexural test results.

Specimen label	Peak load P_1 (kN)	Flexural strength f_f (MPa)	$f_{L/400}$ (MPa)	$f_{L/300}$ (MPa)	$f_{L/150}$ (MPa)	$f_{L/100}$ (MPa)	$T_{L/400}$ (J)	$T_{L/300}$ (J)	$T_{L/150}$ (J)	$T_{L/100}$ (J)
M1–1	17.1	5.1	0.0	0.0	0.0	0.0	3.5	0.0	0.0	0.0
M1–2	15.4	4.6	0.0	0.0	0.0	0.0	3.1	0.0	0.0	0.0
M1–3	15.6	4.7	0.0	0.0	0.0	0.0	2.8	0.0	0.0	0.0
Mean	16.0	4.8	0.0	0.0	0.0	0.0	3.1	3.1	3.1	3.1
SD	0.9	0.3	0.0	0.0	0.0	0.0	0.4	0.0	0.0	0.0
M2–1	20	6.0	4.6	2.6	0.9	0.5	8.6	11.3	16.3	18.4
M2–2	14	4.2	3.1	2.4	0.6	0.3	6.1	8.4	13.3	15.0
M2–3	19	5.7	3.1	1.9	0.7	0.3	6.3	8.3	12.3	14.0
Mean	17.7	5.3	3.6	2.3	0.7	0.4	7.0	9.3	14.0	15.8
SD	3.2	1.0	0.9	0.3	0.1	0.1	1.4	1.7	2.1	2.3
M3–1	17.3	5.2	5.2	4.6	2.5	1.6	6.0	10.1	21.2	28.0
M3–2	18.5	5.6	5.5	5.1	3.5	2.0	7.4	11.8	26.0	34.9
M3–3	18.5	5.6	5.6	5.2	3.2	2.0	9.1	13.6	27.6	36.1
Mean	18.1	5.4	5.4	5.0	3.1	1.9	7.5	11.8	24.9	33.0
SD	0.7	0.2	0.2	0.3	0.5	0.2	1.6	1.8	3.3	4.4
M4–1	19.3	5.8	2.5	1.7	0.8	0.3	6.8	8.5	12.4	14.0
M4–2	17.6	5.3	3.4	2.9	0.9	0.4	6.9	9.5	15.5	17.6
M4–3	16.8	5.0	2.5	2.0	0.4	0.2	6.5	8.3	11.6	12.3
Mean	17.9	5.4	2.8	2.2	0.7	0.3	6.7	8.8	13.2	14.6
SD	1.3	0.4	0.5	0.6	0.3	0.1	0.2	0.6	2.1	2.7
M5–1	13.5	4.1	3.5	3.1	1.4	0.5	6.6	9.3	16.2	19.2
M5–2	14.6	4.4	4.4	4.0	2.5	1.3	6.8	10.3	21.2	27.3
M5–3	13.2	4.0	3.6	3.2	1.4	0.7	5.8	8.7	16.0	19.2
Mean	13.8	4.2	3.8	3.4	1.7	0.9	6.4	9.4	17.8	21.9
SD	0.7	0.2	0.5	0.5	0.6	0.4	0.5	0.8	2.9	4.7

Note: "SD": Standard Deviation; "$f_{L/400}$, $f_{L/300}$, $f_{L/150}$, and $f_{L/100}$": residual flexural strengths at the deflections of $L/400$ (0.75 mm), $L/300$ (1 mm), $L/150$ (2 mm), $L/100$ (3 mm), respectively; "$T_{L/400}$, $T_{L/300}$, $T_{L/150}$, and $T_{L/100}$": flexural toughnesses at the deflections of $L/400$, $L/300$, $L/150$, $L/100$, respectively.

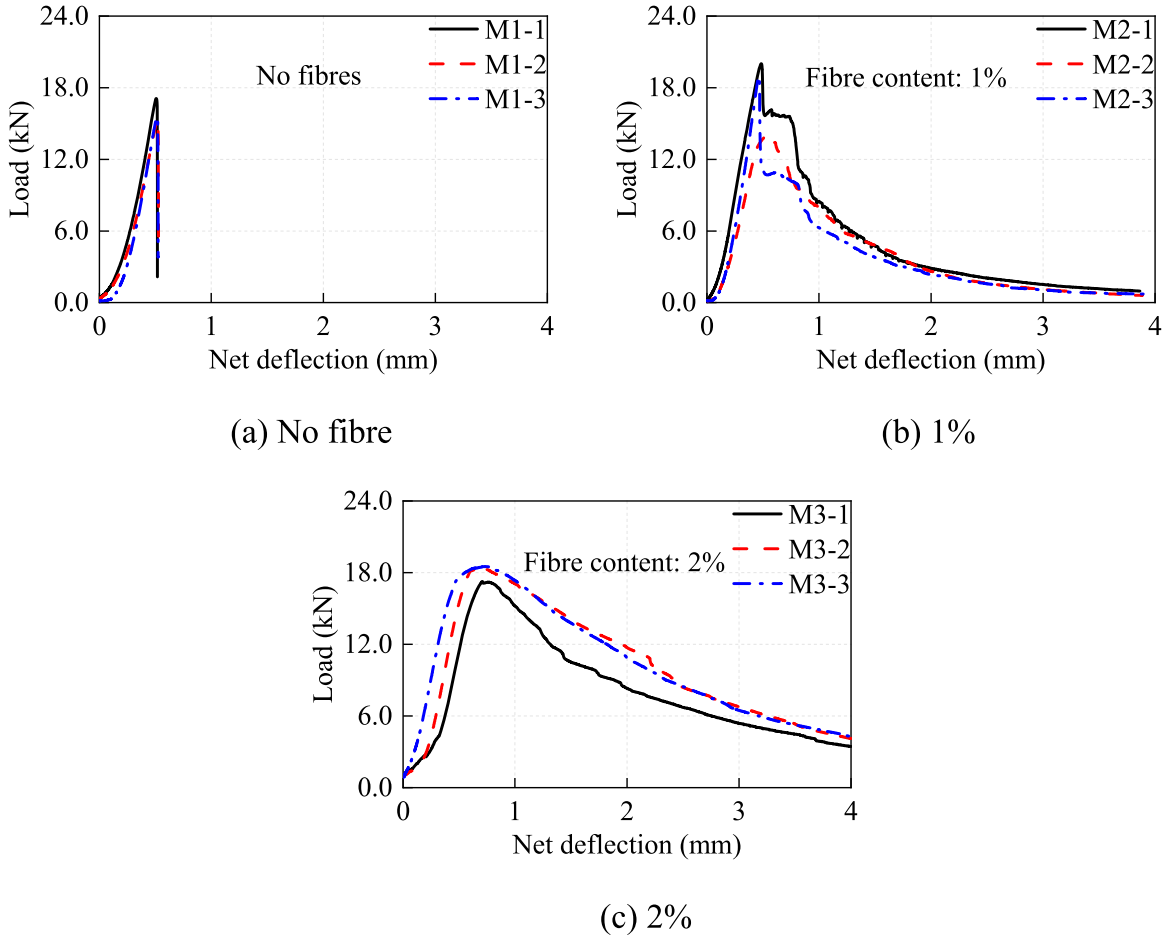

Fig. 15. Comparison of the flexural load-deflection curves of GPC specimens with different fibre contents.

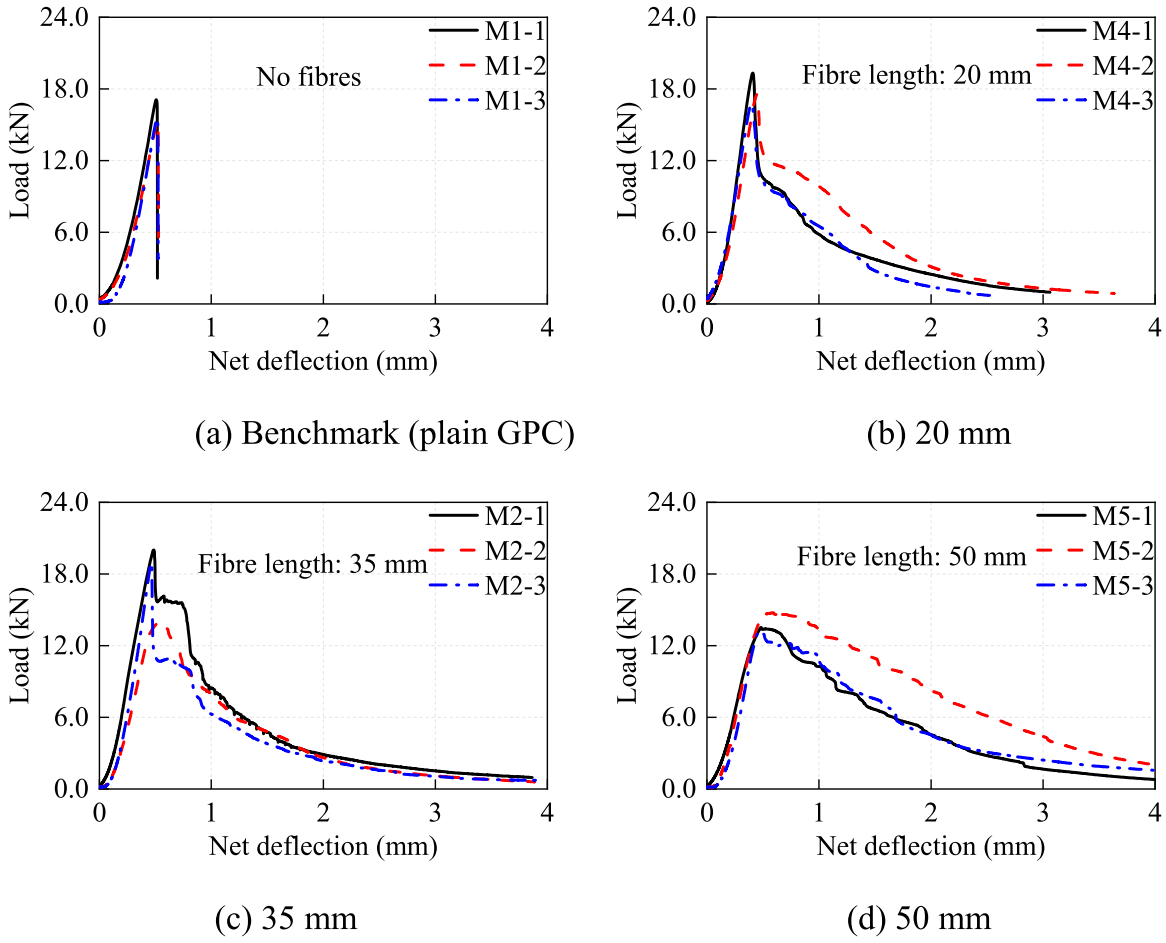

Fig. 16. Comparison of the flexural load-deflection curves of GPC specimens with different fibre lengths.

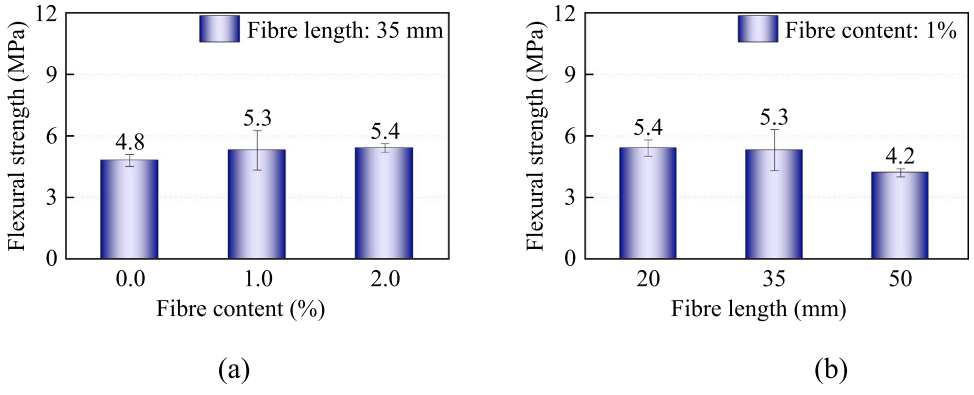

Fig. 17. Effects of fibre content (a) and fibre length (b) on the flexural strength f_f of GPC specimens.

than that of fibre length.

3.5.5. *Flexural toughness and index*

The flexural toughness T_f at different deflections ($T_{f,L/400}$, $T_{f,L/300}$, $T_{f,L/150}$, and $T_{f,L/100}$) is defined as the area under the load-deflection curve up to a specified net deflection [31], with the test results shown in Fig. 20. Similar to the compressive toughness index I_c, the flexural toughness index I_f could also be defined as the ratio of the toughness of fibre reinforced concrete to that of concrete without fibres [47]. The test results show that the fibre content and fibre length have positive effects on the flexural toughness and flexural toughness index. The flexural toughness T_f and flexural toughness index I_f of plain GPC remained 3.1 J (black solid line, see Fig. 20(a)) and 1 (black solid line, see Fig. 20(b)), respectively, due to little post-cracking resistance of plain GPC. For flexural toughness T_f at a net deflection of $L/100$ as shown in Fig. 20(a), the p-values for specimens with $V_f = 0$ % vs. 1 %, $V_f = 0$ % vs. 2 %, and $V_f = 1$ % vs. 2 % are 0.0006, 0.0003, and 0.0039 (all less than 0.05), respectively, which are considered statistically significant and clearly indicate the effect of fibre content on the flexural toughness of BMF-GPC. As observed, GPC with 2 % 35 mm-long BMFs had higher flexural toughness and flexural toughness index at $L/100$ than plain GPC by up to 965 %. As shown in Fig. 20(c) and (d), GPC with 1 % 50 mm-long BMFs had higher flexural toughness and flexural toughness index than plain GPC by up to 606 %. The test results indicate a

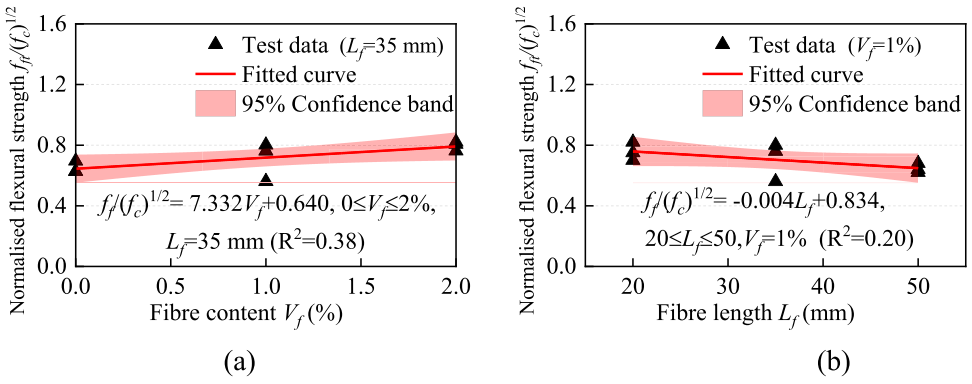

Fig. 18. Effects of (a) fibre content and (b) fibre length on the normalised flexural strength $f_f/(f_c)^{1/2}$ of GPC specimens.

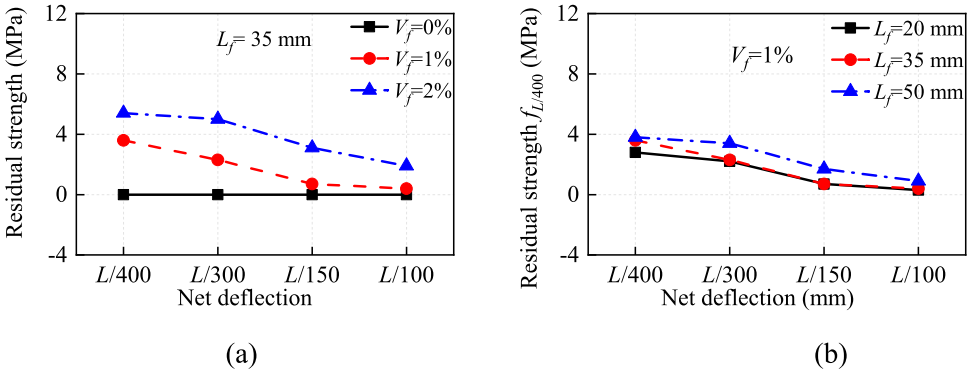

Fig. 19. Effects of (a) fibre content and (b) fibre length on the residual strengths of GPC specimens.

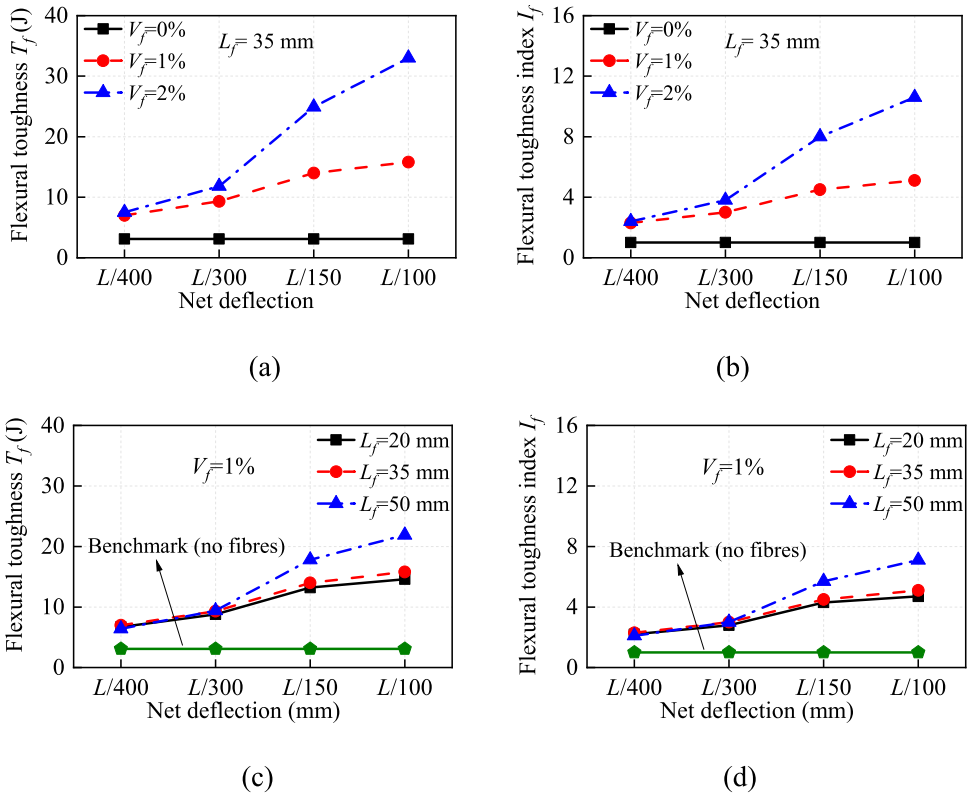

Fig. 20. Effects of (a) & (b) fibre content and (c) & (d) fibre length on the flexural toughness T_f and flexural toughness index I_f of GPC specimens, respectively.

significantly improved energy absorption capacity of BMF-GPC as compared to plain GPC.

4. Conclusions

In this study, a new type of basalt macro fibres (BMFs)-reinforced geopolymer concrete (GPC), denoted as BMF-GPC, was developed and its mechanical properties were investigated. The effects of fibre content and fibre length on the mechanical properties of GPC were revealed. The results were analysed and discussed in terms of slump, modulus of elasticity, compressive strength, compressive stress-strain curve, peak strain (strain corresponding to peak stress), compressive toughness and index, flexural load-deflection curve, flexural and residual strengths, and flexural toughness and index. Based on the test results, the following conclusions can be drawn.

1. The slump of GPC decreased by up to 36 % with increasing fibre content from 0 % to 2 %, whilst it only slightly decreased by 6 % with increasing fibre length from 20 mm to 50 mm. The effect of fibre length on the workability of GPC is insignificant.
2. The fibre content and fibre length exerted limited effects on the modulus of elasticity of GPC.
3. Higher fibre content and fibre length led to a more ductile post-peak strain softening of compressive stress-strain curve and higher peak strains. Both the compressive toughness and compressive toughness index of BMF-GPC increased by up to 126 % with the addition of 2 % 35 mm-long BMFs as compared to GPC.
4. An analytical model was proposed to predict the compressive stress-strain behaviour of BMF-GPC. This model takes into account the effects of both BMF content and length, and demonstrated a good agreement with the test results. It could be used for the design of GPC/BMF-GPC structures.
5. With the addition of 2 % 35 mm-long BMFs, the flexural strength of BMF-GPC was only improved by 13 %. However, the flexural toughness and flexural toughness index were greatly improved by up to 965 %.
6. Increasing BMF content and length leads to better compressive and flexural performances of BMF-GPC, especially the compressive and flexural toughness (energy absorption capacities). The effect of fibre content on its performance is more prominent than that of fibre length.

CRediT authorship contribution statement

Zhijie Huang: Writing – original draft, Methodology, Investigation, Formal analysis, Data curation, Conceptualization. **Cek Sem So:** Investigation, Data curation. **Wensu Chen:** Writing – review & editing, Validation, Supervision, Project administration, Methodology, Conceptualization. **Paing Min Htet:** Writing – review & editing, Investigation. **Hong Hao:** Writing – review & editing, Validation, Supervision, Funding acquisition, Conceptualization.

Declaration of Competing Interest

The authors declare that they have no known competing financial interests or personal relationships that could have appeared to influence the work reported in this paper.

Data Availability

Data will be made available on request.

Acknowledgements

The authors are thankful for the financial support from Australian Research Council (ARC) under the Australian Laureate Fellowship (FL180100196).

References

[1] H. Hao, K. Bi, W. Chen, T.M. Pham, J. Li, Towards next generation design of sustainable, durable, multi-hazard resistant, resilient, and smart civil engineering structures, Eng. Struct. 277 (2023) 115477.
[2] Z. Huang, W. Chen, H. Hao, R. Aurelio, Z. Li, T.M. Pham, Test of dynamic mechanical properties of ambient-cured geopolymer concrete using split hopkinson pressure bar, J. Mater. Civ. Eng. 34 (2022) 04021440.
[3] N. Li, C. Shi, Z. Zhang, H. Wang, Y. Liu, A review on mixture design methods for geopolymer concrete, Compos Part B Eng. 178 (2019).
[4] W. Chen, Q. Wang, Z. Huang, H. Du, Hydration mechanism and mechanical properties of a developed low-carbon and lightweight strain-hardening cementitious composites, J. Sustain. Cem. Based Mater. (2023) 1–17.
[5] H. Jamshaid, R. Mishra, A green material from rock: basalt fiber–a review, J. Text. Inst. 107 (2016) 923–937.
[6] V. Dhand, G. Mittal, K.Y. Rhee, S.-J. Park, D. Hui, A short review on basalt fiber reinforced polymer composites, Compos Part B Eng. 73 (2015) 166–180.
[7] Y. Li, J. Zhang, Y. He, G. Huang, J. Li, Z. Niu, et al., A review on durability of basalt fiber reinforced concrete, Compos Sci. Technol. 225 (2022).
[8] G. Wu, X. Wang, Z. Wu, Z. Dong, G. Zhang, Durability of basalt fibers and composites in corrosive environments, J. Compos Mater. 49 (2015) 873–887.
[9] J. Branston, S. Das, S.Y. Kenno, C. Taylor, Mechanical behaviour of basalt fibre reinforced concrete, Constr. Build. Mater. 124 (2016) 878–886.
[10] J. Shi, Y. Lu, R. Zhu, Y. Liu, Y. Zhang, Q. Lv, Experimental evaluation of fracture toughness of basalt macro fiber reinforced high performance lightweight aggregate concrete, Constr. Build. Mater. 411 (2024).
[11] Q. Wang, Y. Ding, Y. Zhang, C. Castro, Effect of macro polypropylene fiber and basalt fiber on impact resistance of basalt fiber-reinforced polymer-reinforced concrete, Struct. Concr. 22 (2021) 503–515.
[12] Z. Huang, W. Chen, H. Hao, A.U. Siew, T. Huang, M. Ahmed, et al., Lateral impact performances of geopolymer concrete columns reinforced with steel-BFRP composite bars, Constr. Build. Mater. 411 (2024) 134411.
[13] A. El Refai, W. Alnahhal, A. Al-Hamrani, S. Hamed, Shear performance of basalt fiber-reinforced concrete beams reinforced with BFRP bars, Compos Struct. 288 (2022).
[14] M.G. Sohail, W. Alnahhal, A. Taha, K. Abdelaal, Sustainable alternative aggregates: characterization and influence on mechanical behavior of basalt fiber reinforced concrete, Constr. Build. Mater. 255 (2020).
[15] W. Alnahhal, R. Taha, N. Alnuaimi, A. Al-Hamrani, Properties of fibre-reinforced concrete made with discarded materials, Mag. Concr. Res. 71 (2019) 152–162.
[16] Adhikari S. Mechanical and structural characterization of mini-bar reinforced concrete beams: University of Akron, 2013.
[17] C. Zhang, H. Hao, Y. Hao, Experimental study of mechanical properties of double-helix BFRP fiber reinforced concrete at high strain rates, Cem. Concr. Compos (2022) 104633.
[18] S. Shoaib, T. El-Maaddawy, H. El-Hassan, B. El-Ariss, M. Alsalami, Fresh and hardened properties of concrete reinforced with basalt macro-fibers, Buildings 12 (2022).
[19] S. Shoaib, T. El-Maaddawy, H. El-Hassan, B. El-Ariss, M. Alsalami, Characteristics of basalt macro-fiber reinforced recycled aggregate concrete, Sustainability 14 (2022).
[20] H. Abbas Ashour Alaraza, M. Kharun, P.C. Chiadighikaobi, The effect of minibars basalt fiber fraction on mechanical properties of high-performance concrete, Cogent Eng. 9 (2022).
[21] Z. Chen, X. Wang, L. Ding, K. Jiang, X. Liu, J. Liu, et al., Spalling resistance and mechanical properties of ultra-high performance concrete reinforced with multi-scale basalt fibers and hybrid fibers under elevated temperature, J. Build. Eng. 77 (2023).
[22] Z. Chen, X. Wang, L. Ding, K. Jiang, C. Su, J. Liu, et al., Mechanical properties of a novel UHPC reinforced with macro basalt fibers, Constr. Build. Mater. 377 (2023).
[23] G. Furtos, D. Prodan, C. Sarosi, M. Moldovan, K. Korniejenko, L. Miller, et al., Mechanical properties of minibars basalt fiber-reinforced geopolymer composites, Materials 17 (2024).
[24] AS/NZS 3582.1. Supplementary cementitious materials, Part 1: Fly ash. Australia/New Zealand: Standards Australia / Standards New Zealand; 2016.
[25] AS 3582.2. Supplementary cementitious materials, Part 2: Slag - Ground granulated blast-furnace. Sydney, NSW, Australia: Standards Australia; 2016.
[26] S. Sharmin, P.K. Sarker, W.K. Biswas, R.M. Abousnina, U. Javed, Characterization of waste clay brick powder and its effect on the mechanical properties and microstructure of geopolymer mortar, Constr. Build. Mater. 412 (2024) 134848.
[27] W. Alnahhal, O. Aljidda, Flexural behavior of basalt fiber reinforced concrete beams with recycled concrete coarse aggregates, Constr. Build. Mater. 169 (2018) 165–178.
[28] ASTM C143, Standard Test Method for Slump of Hydraulic-Cement Concrete, ASTM International, West Conshohocken, PA, USA, 2015.
[29] ASTM C39, Standard Test Method for Compressive Strength of Cylindrical Concrete Specimens, ASTM International, West Conshohocken, PA, USA, 2020.
[30] ASTM C469, Standard Test Method for Static Modulus of Elasticity and Poisson's Ratio of Concrete in Compression, ASTM International, West Conshohocken, PA, USA, 2014.
[31] ASTM C1609, Standard Test Method for Flexural Performance of Fiber-Reinforced Concrete (Using Beam With Third-Point Loading), ASTM International, West Conshohocken, PA, USA, 2019.

[32] A. Noushini, M. Hastings, A. Castel, F. Aslani, Mechanical and flexural performance of synthetic fibre reinforced geopolymer concrete, Constr. Build. Mater. 186 (2018) 454–475.
[33] H. Zhang, P.K. Sarker, Q. Wang, B. He, Z. Jiang, Strength and toughness of ambient-cured geopolymer concrete containing virgin and recycled fibres in mono and hybrid combinations, Constr. Build. Mater. 304 (2021).
[34] A. Patnaik, L. Miller, S. Adhikari, P.C. Standal, Basalt FRP minibar reinforced concrete, Fibre Concr. (2013) 12–13.
[35] T.K. Kim, T test as a parametric statistic, Korean J. Anesthesiol. 68 (2015) 540.
[36] M.A. Khasawneh, A.A. Sawalha, M.T. Aljarrah, M.A. Alsheyab, Effect of aggregate gradation and asphalt mix volumetrics on the thermal properties of asphalt concrete, Case Stud. Constr. Mater. 18 (2023) e01725.
[37] J. Carrillo, J. Ramirez, J. Lizarazo-Marriaga, Modulus of elasticity and Poisson's ratio of fiber-reinforced concrete in Colombia from ultrasonic pulse velocities, J. Build. Eng. 23 (2019) 18–26.
[38] J.S. Volz, K.H. Khayat, M. Arezoumandi, J. Drury, S. Sadati, A. Smith, et al., Recycled Concrete Aggregate (RCA) for Infrastructure Elements, Missouri University of Science and Technology, Rolla, Missouri, USA, 2014.
[39] C. Wirkman, Performance of Fiber-Reinforced Self-Consolidating Concrete for Repair of Bridge Sub-Structures, University of Oklahoma, Norman, Oklahoma, USA, 2016.
[40] SA TS 199:2023, Design of Geopolymer and Alkali-activated Binder Concrete Structures, Standards Australia, Sydney, Australia, 2023.
[41] ACI 318-14, Building Code Requirements for Structural Concrete (ACI 318-14) and Commentary on Building Code Requirements for Structural Concrete (ACI 318-14), American Concrete Institute, Farmington Hills, MI, USA, 2014.
[42] Z. Huang, W. Chen, H. Hao, Z. Chen, T.M. Pham, T.T. Tran, et al., Shear behaviour of ambient cured geopolymer concrete beams reinforced with BFRP bars under static and impact loads, Eng. Struct. 231 (2021) 111730.
[43] Z. Huang, M.Z.N. Khan, W. Chen, H. Hao, M. Elchalakani, T.M. Pham, Effectiveness of reinforcing methods in enhancing the lateral impact performance of geopolymer concrete column reinforced with BFRP bars, Int. J. Impact Eng. 175 (2023) 104544.
[44] Z. Huang, M.Z.N. Khan, W. Chen, H. Hao, Y. Wu, T.M. Pham, et al., Experimental and numerical study of the performance of geopolymer concrete columns reinforced with BFRP bars subjected to lateral impact loading, Constr. Build. Mater. 357 (2022) 129362.
[45] C.S. Poon, Z.H. Shui, L. Lam, Compressive behavior of fiber reinforced high-performance concrete subjected to elevated temperatures, Cem. Concr. Res. 34 (2004) 2215–2222.
[46] M. Nematzadeh, A. Salari, J. Ghadami, M. Naghipour, Stress-strain behavior of freshly compressed concrete under axial compression with a practical equation, Constr. Build. Mater. 115 (2016) 402–423.
[47] M. Mansur, M. Chin, T. Wee, Stress-strain relationship of high-strength fiber concrete in compression, J. Mater. Civ. Eng. 11 (1999) 21–29.
[48] S. Popovics, A numerical approach to the complete stress-strain curve of concrete, Cem. Concr. Res. 3 (1973) 583–599.
[49] D.J. Carreira, K.-H. Chu, Stress-strain relationship for plain concrete in compression, J. Proc. (1985) 797–804.
[50] M. Nataraja, N. Dhang, A. Gupta, Stress–strain curves for steel-fiber reinforced concrete under compression, Cem. Concr. Compos 21 (1999) 383–390.
[51] F. Bencardino, L. Rizzuti, G. Spadea, R.N. Swamy, Stress-strain behavior of steel fiber-reinforced concrete in compression, J. Mater. Civ. Eng. 20 (2008) 255–263.
[52] A.K. Samani, M.M. Attard, A stress–strain model for uniaxial and confined concrete under compression, Eng. Struct. 41 (2012) 335–349.
[53] Y. Chi, L. Xu, Y. Zhang, Experimental study on hybrid fiber–reinforced concrete subjected to uniaxial compression, J. Mater. Civ. Eng. 26 (2014) 211–218.
[54] M. Nematzadeh, F. Hasan-Nattaj, Compressive stress-strain model for high-strength concrete reinforced with forta-ferro and steel fibers, J. Mater. Civ. Eng. 29 (2017).
[55] Y. Wang, W. Long, Complete stress–strain curves for pine needle fibre reinforced concrete under compression, Constr. Build. Mater. 302 (2021).
[56] F. Shi, T.M. Pham, H. Hao, Y. Hao, Post-cracking behaviour of basalt and macro polypropylene hybrid fibre reinforced concrete with different compressive strengths, Constr. Build. Mater. 262 (2020).
[57] M. Arezoumandi, A.R. Steele, J.S. Volz, Evaluation of the bond strengths between concrete and reinforcement as a function of recycled concrete aggregate replacement level, Struct. Elsevier (2018) 73–81.
[58] M. Arezoumandi, C.A. Ortega, J.S. Volz, Flexural behavior of high-volume fly ash concrete beams: experimental study, Transp. Res. Rec. 2508 (2015) 22–30.
[59] A.A. Ghadban, N.I. Wehbe, M. Underberg, Effect of fiber type and dosage on flexural performance of fiber-reinforced concrete for highway bridges, Acids Mater. J. 115 (2018).